Rovibronic analysis of the Jahn–Teller effect in CH2D2+ at low energies

Author(s):
Grütter, Michel; Wörner, Hans Jakob; Merkt, Frédéric

Publication date:
2009-07-14

Permanent link:
https://doi.org/10.3929/ethz-a-010782536

Originally published in:
The Journal of Chemical Physics 131(2), https://doi.org/10.1063/1.3157210

The following article appeared in *J. Chem. Phys.* **131**, 024309 (2009) and may be found at http://dx.doi.org/10.1063/1.3157210.

Rovibronic analysis of the Jahn–Teller effect in CH 2 D 2 + at low energies

M. Grütter, H. J. Wörner, and F. Merkt

Citation: The Journal of Chemical Physics **131**, 024309 (2009); doi: 10.1063/1.3157210
View online: http://dx.doi.org/10.1063/1.3157210
View Table of Contents: http://scitation.aip.org/content/aip/journal/jcp/131/2?ver=pdfcov
Published by the AIP Publishing

Rovibronic analysis of the Jahn–Teller effect in $CH_2D_2^+$ at low energies

M. Grütter,[1] H. J. Wörner,[2] and F. Merkt[1,a)]
[1]*Laboratorium für Physikalische Chemie, ETH Zürich, CH-8093 Zurich, Switzerland*
[2]*NRC Steacie Institute for Molecular Sciences, Ottawa, Ontario K1A 0R6, Canada*

(Received 27 April 2009; accepted 30 May 2009; published online 14 July 2009)

The Jahn–Teller effect in the ground state of $CH_2D_2^+$ has been studied by pulsed-field-ionization zero-kinetic-energy photoelectron spectroscopy. The lowest three bands have been assigned to the three isomers $CH_\ell H_\ell D_s D_s^+$, $CH_\ell H_s D_\ell D_s^+$, and $CH_s H_s D_\ell D_\ell^+$, in which the deuterium atoms are attached to the central carbon atom by two short bonds, one short and one long bond, and two long bonds, respectively, and which have different zero-point vibrational energies. Whereas $CH_\ell H_\ell D_s D_s^+$ and $CH_s H_s D_\ell D_\ell^+$ can each be described by a single structure with C_{2v} symmetry, $CH_\ell H_s D_\ell D_s^+$ corresponds to four equivalent C_1 structures that interconvert by tunneling. The rotational structure of these three bands is compared with predictions made on the basis of a tunneling Hamiltonian combined with a rotational Hamiltonian that incorporates the effects of the large-amplitude tunneling motion. The zero-point energies of $CH_\ell H_s D_\ell D_s^+$ and $CH_s H_s D_\ell D_\ell^+$ relative to that of $CH_\ell H_\ell D_s D_s^+$ are $\Delta = 123.6(5)\ \mathrm{cm}^{-1}$ and $\Delta' = 243.2(5)\ \mathrm{cm}^{-1}$, respectively, and the tunneling matrix element σ coupling the four C_{2v} equilibrium structures of $CH_\ell H_s D_\ell D_s^+$ is $-1.7(4)\ \mathrm{cm}^{-1}$.
 [DOI: 10.1063/1.3157210]

I. INTRODUCTION

The Jahn–Teller effect in molecules with high permutational symmetry is often accompanied by the existence of many equivalent distorted minimum energy structures connected by a network of tunneling paths through low-lying barriers on the potential energy surfaces.[1–4] Large-amplitude tunneling motions become important and the molecular structure must be thought of as being fluxional; a high density of low-lying vibronic (tunneling) levels and a complex rovibrational energy level structure result.

The methane cation represents a prototypical molecular system with which this complexity and the underlying large-amplitude motions can be studied in detail experimentally and theoretically. With only nine electrons, CH_4^+ can in principle be studied very accurately by *ab initio* quantum chemistry and, indeed, many insights have been gained from such studies (see, e.g., Refs. 4–6). Studies of the nine-dimensional nuclear motion on the three electronic potential surfaces arising from the triply degenerate ground state still represent a challenge, but recent progress in vibrational calculations in molecular systems of similar complexity suggests that an adequate treatment may become available soon.[7,8] Photoelectron spectroscopy of CH_4 and its deuterated isotopomers in the gas phase[9–17] and electron paramagnetic resonance (EPR) spectroscopy of CH_4^+ and its deuterated isotopomers in rare gas matrices[18–20] have been the main spectroscopic methods with which information on the methane cation has been obtained experimentally.

From these theoretical and experimental studies, the following overall picture of the structural and spectral properties of the methane cation emerged: The minimum energy structure is of C_{2v} point group symmetry with two short C–H(D) bonds separated by a large angle and two long C–H(D) bonds separated by a small angle.[4–6,12,13] Twelve such equivalent structures exist, which can be treated as two enantiomeric sets of six structures each.[4,6,13,21] Zero-point energy effects favor structures in which the D atoms are located on short bonds and, therefore, successive deuteration has a large effect on the structure and tunnel dynamics of the methane cation. Whereas the ground state of CH_4^+ is delocalized over six equivalent potential wells and splits into two (T_2 and T_1) vibronic components separated by a tunneling splitting of about $16\ \mathrm{cm}^{-1}$,[15] the ground state of $CH_2D_2^+$ is localized in a single potential well and can be approximately described as a rigid rotor.[12] On the basis of a one-dimensional pseudorotational model, three isomers of $CH_2D_2^+$ were predicted in Ref. 13, corresponding to structures with the H atoms located both on the long bonds, one on a long and one on a short bond, and both on the short bonds. In CH_3D^+ and CD_3H^+, the Jahn–Teller effect gives rise to two energetically distinguishable isomeric forms in which either one or two of the three equivalent ligand atoms are located on a short bond.[13,17,21]

High-resolution pulsed-field-ionization zero-kinetic-energy (PFI-ZEKE) photoelectron spectra of jet-cooled CH_4, CH_3D, CH_2D_2, CD_3H, and CD_4 only display a band structure in a narrow energy range above the adiabatic ionization threshold. Beyond $500\ \mathrm{cm}^{-1}$ of internal energy in the cation, this band structure evolves into an uninterrupted dense sequence of sharp lines.[13] The band structure at low energies could be analyzed, first partially in terms of a one-dimensional tunneling model,[13] and then fully using an effective vibronic tunneling Hamiltonian formalism based on a group-theoretical treatment.[15–17,21] Reference 21 contains a detailed discussion of the isomerism in CH_3D^+ and CD_3H^+ mentioned above and predicts the existence of chiral isomers

a)Electronic mail: feme@xuv.phys.chem.ethz.ch.

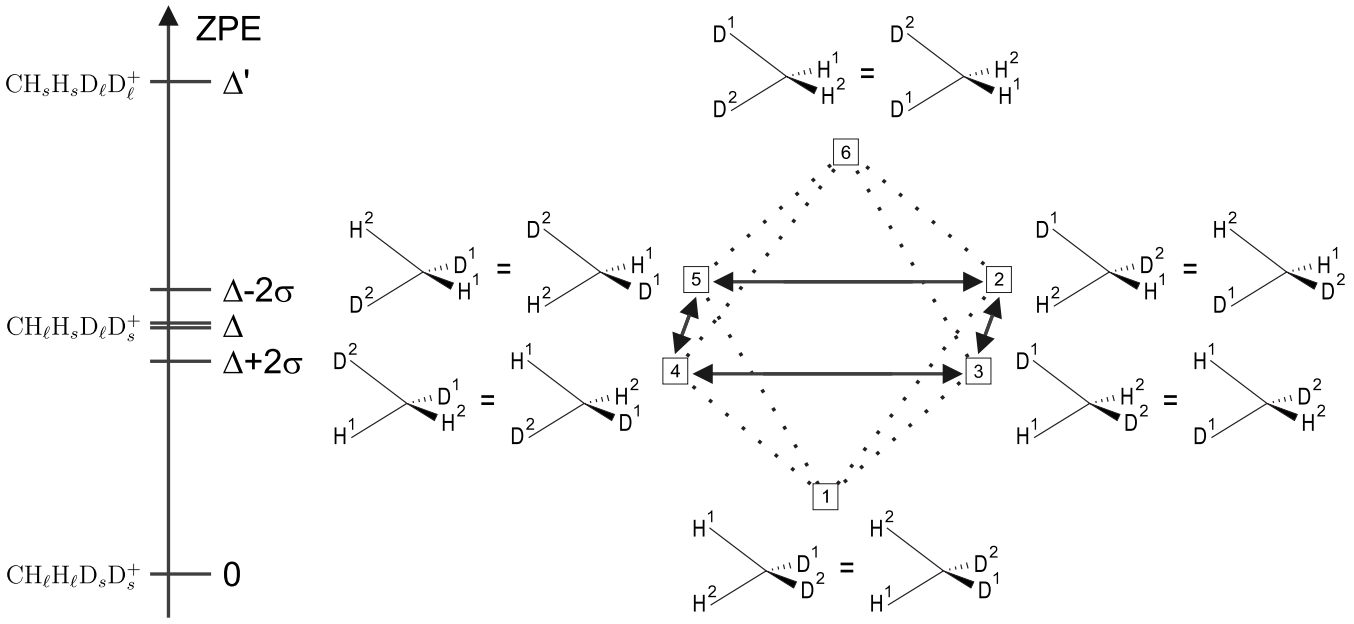

FIG. 1. Schematic representation of one of the two enantiomeric sets of six equivalent minimum energy structures on the ground-state potential energy hypersurface of the methane cation and of the network of tunneling paths connecting them. The dotted tunneling paths interconvert the $CH_\ell H_\ell D_sD_s^+$, $CH_\ell H_sD_\ell D_s^+$, and $CH_sH_sD_\ell D_\ell^+$ isomeric forms of $CH_2D_2^+$, which have different zero-point vibrational energies, whereas the full double arrows indicate interconversion of equivalent structures of the $CH_\ell H_sD_\ell D_s^+$ isomeric form. The energy scale on the left-hand side indicates schematically the relative order of the zero-point energies of the three isomeric forms and the tunneling splittings of $CH_\ell H_sD_\ell D_s^+$ (see text for more detail). Each structure was drawn twice to facilitate the comparison of the different isomeric forms.

of $CH_2D_2^+$ (see Fig. 18 of Ref. 21). Incorporating the rotational motion in this vibronic tunneling model enabled the analysis of the rotational-tunneling energy level structure of the first vibronic states of CH_4^+,[15] CD_4^+,[16] CH_3D^+, and CD_3H^+.[17] However, it turned out to be impossible to derive compact analytical expressions for the rotational Hamiltonian of $CH_2D_2^+$.

In the present article, we extend our formalism so that the rotational structure of $CH_2D_2^+$ can also be treated and use the resulting expressions to analyze the rotational structure of the lowest three bands in the PFI-ZEKE photoelectron spectrum of CH_2D_2. The lowest two bands of this spectrum have already been shown in Fig. 8d of Ref. 13 with a vibronic assignment made in the realm of a one-dimensional pseudorotational model and the rotational structure of the lowest one could be analyzed in Ref. 12. The main results of the present investigation concern the rotational structure of the second and third bands of the PFI-ZEKE photoelectron spectrum of CH_2D_2. These results lend support to the predictions of three isomeric forms of $CH_2D_2^+$ made in Refs. 13 and 21. The new results on $CH_2D_2^+$, when combined with those obtained on CH_4^+, $^{13}CH_4^+$, CD_4^+, CH_3D^+, and CD_3H^+ [15–17,21] provide a global interpretation of the structural properties of the methane cation at low energies.

II. EXPERIMENT

The PFI-ZEKE photoelectron spectra of CH_2D_2, the lowest two bands of which were already presented in Refs. 12 and 13, were recorded using the spectrometer described in Ref. 11 following single-photon excitation from the neutral ground state. Vacuum ultraviolet (VUV) radiation, tunable in the range 101 800–102 100 cm^{-1}, was generated by resonance-enhanced four-wave mixing in Xe using two dye lasers. The frequency-doubled output of the first laser was fixed at the position of the two-photon resonance ($2\tilde{\nu}_1$=80 118.9839 cm^{-1}) of atomic Xe and the wave number $\tilde{\nu}_2$ of the second laser was scanned to produce the tunable VUV radiation of wave number $2\tilde{\nu}_1+\tilde{\nu}_2$. The VUV beam was separated from the beams of wave numbers $\tilde{\nu}_1$ and $\tilde{\nu}_2$ using a grating monochromator. The VUV laser beam intersected a pulsed supersonic beam of CH_2D_2 (Cambridge Isotope Laboratories, 98% chemical purity, 98% isotopic enrichment). The photoelectron spectrum was obtained by monitoring, as a function of the VUV wave number, the yield of electrons produced by the pulsed electric field ionization of high Rydberg states. An electric-field pulse sequence consisting of two successive pulses was employed, which led to a resolution of 0.6 cm^{-1}.

III. THEORETICAL TREATMENT OF THE JAHN–TELLER EFFECT IN $CH_2D_2^+$

A. Vibronic tunneling Hamiltonian

The vibronic Hamiltonian, $\hat{H}_{tun}$, which describes the tunneling motion of the six lowest vibronic states of $CH_2D_2^+$ has been derived in Ref. 21 following the same procedure as in the cases of CH_4^+,[15] CD_4^+,[16] CH_3D^+, and CD_3H^+.[17] The 12 equivalent C_{2v} minimum energy structures on the potential energy hypersurface of CH_4^+ form two enantiomeric sets of six structures, each connected by a network of tunneling paths. Because the potential barrier separating enantiomeric structures is high, it is sufficient, at low energies, to only consider the interconversion of structures by tunneling within a given enantiomeric set. The six structures are displayed in Fig. 1 at the vertices of the octahedron that is used

to discuss the tunneling motion of CH_4^+.[6,13,21] The dotted lines and full arrows representing the edges of this octahedron correspond to the possible tunneling processes.

In $CH_2D_2^+$, the six structures displayed in Fig. 1 have different zero-point vibrational energies: The structure having two short C–D bonds ($CH_\ell H_\ell D_s D_s^+$, structure 1 in Fig. 1) has the lowest zero-point energy; the four structures with one short and one long C–D bond ($CH_\ell H_s D_\ell D_s^+$, structures 2–5 in Fig. 1) have the same intermediate zero-point energy. The structure with two long C–D bonds ($CH_s H_s D_\ell D_\ell^+$, structure 6 in Fig. 1) has the highest zero-point energy. Consideration of these three different types of isomeric structures and of the tunneling paths between them leads to the tunneling Hamiltonian,[21]

$$\mathbf{H}_{\text{tun}} = \begin{pmatrix} 0 & \sigma' & -\sigma' & \sigma' & -\sigma' & 0 \\ \sigma' & \Delta & \sigma & 0 & -\sigma & \sigma'' \\ -\sigma' & \sigma & \Delta & -\sigma & 0 & \sigma'' \\ \sigma' & 0 & -\sigma & \Delta & \sigma & \sigma'' \\ -\sigma' & -\sigma & 0 & \sigma & \Delta & \sigma'' \\ 0 & \sigma'' & \sigma'' & \sigma'' & \sigma'' & \Delta' \end{pmatrix} \cong \begin{pmatrix} 0 & 0 & 0 & 0 & 0 & 0 \\ 0 & \Delta & \sigma & 0 & -\sigma & 0 \\ 0 & \sigma & \Delta & -\sigma & 0 & 0 \\ 0 & 0 & -\sigma & \Delta & \sigma & 0 \\ 0 & -\sigma & 0 & \sigma & \Delta & 0 \\ 0 & 0 & 0 & 0 & 0 & \Delta' \end{pmatrix}. \quad (1)$$

The matrix elements $\langle \phi_n | \hat{H}_{\text{tun}} | \phi_n \rangle$ in Eq. (1) were evaluated using the basis functions $\phi_n = |n\rangle|\chi_n\rangle$, which represent products of the adiabatic electronic functions $|n\rangle$ for each minimum energy structure [i.e., $(1/\sqrt{2})(|\eta\rangle - |\zeta\rangle)$, $(1/\sqrt{2})(|\xi\rangle + |\eta\rangle)$, $(1/\sqrt{2})(|\xi\rangle + |\zeta\rangle)$, $(1/\sqrt{2})(-|\xi\rangle + |\eta\rangle)$, $(1/\sqrt{2})(-|\xi\rangle + |\zeta\rangle)$, and $(1/\sqrt{2})(|\eta\rangle + |\zeta\rangle)$ for wells 1–6, where $|\xi\rangle$, $|\eta\rangle$, and $|\zeta\rangle$ are the three diabatic components of the ground electronic state of CH_4^+ (Ref. 22)] and the vibrational wave functions $|\chi_n\rangle$ described by products of nine ground-state harmonic-oscillator functions.

In Eq. (1), $\sigma'(\sigma'')$ stands for the tunneling coupling element between structure 1 (6) and structures 2–5, and Δ and Δ' for the zero-point energies of structures 2–5 and 6 relative to the zero-point energy of structure 1, respectively. Because Δ and Δ' are much larger (≈ 100 cm^{-1} and ≈ 200 cm^{-1},[13,21] respectively) than the estimated values of σ' and σ'' (in CH_4^+, the tunneling splitting $|\sigma| = \delta/4$ was determined to be ≈ 4 cm^{-1},[15] which represents an upper bound for the values σ' and σ''), σ' and σ'' can be neglected in the determination of the eigenvalues of $\hat{H}_{\text{tun}}$. In this approximation, the eigenvalues of $\hat{H}_{\text{tun}}$ with $\sigma < 0$ are $E_{B_2} = 0$, $E_{A_1} = \Delta + 2\sigma$, $E_{B_1} = E_{B_2} = \Delta$, $E_{A_2} = \Delta - 2\sigma$, and $E_{B_1} = \Delta'$, and the corresponding eigenvectors, which form the columns of the transformation matrix, are $\vec{v}_{B_2} = (1,0,0,0,0,0)$, $\vec{v}_{A_1} = (1/2)(0,-1,-1,1,1,0)$, $\vec{v}_{B_1} = (1/2)(0,1,1,1,1,0)$, $\vec{v}_{B_2} = (1/2)(0,-1,1,-1,1,0)$, $\vec{v}_{A_2} = (1/2)(0,1,-1,-1,1,0)$, and $\vec{v}_{B_1} = (0,0,0,0,0,1)$, respectively.[21] The subscripts used to designate these eigenstates represent their vibronic symmetry in the $C_{2v}(M)$ group.

The vibronic levels cluster in three groups displayed schematically on the left of Fig. 1: The ground state, a group of four closely spaced states with an energy of about Δ and an isolated level of energy Δ'. Whereas the isomers $CH_\ell H_\ell D_s D_s^+$ and $CH_s H_s D_\ell D_\ell^+$ have C_{2v} symmetry, isomers 2–5 have C_1 symmetry but the delocalized eigenstates resulting from the tunneling motions indicated by solid arrows in Fig. 1 can be classified in the $C_{2v}(M)$ molecular symmetry group.[21]

B. Rovibronic problem

With the approximation of Eq. (1), $CH_\ell H_\ell D_s D_s^+$ (labeled I hereafter) and $CH_s H_s D_\ell D_\ell^+$ (III) can be treated as rigid rotors at low J values and their rotational structure described by

$$\frac{\hat{H}_{\text{rot}}^{(1)}}{hc} = A^{\text{I}} \hat{J}_x^2 + C^{\text{I}} \hat{J}_y^2 + B^{\text{I}} \hat{J}_z^2, \quad (2)$$

$$\frac{\hat{H}_{\text{rot}}^{(6)}}{hc} = B^{\text{III}} \hat{J}_x^2 + C^{\text{III}} \hat{J}_y^2 + A^{\text{III}} \hat{J}_z^2, \quad (3)$$

where the superscripts (1) and (6) refer to the structures displayed in Fig. 1. $CH_\ell H_s D_\ell D_s^+$ (II) corresponds to the four structures labeled 2–5 in Fig. 1, which interconvert by tunneling. In order to treat the tunneling-rotational motion of this isomeric form of $CH_2D_2^+$, it is convenient to express the rotational Hamiltonian of structures 2–5 using the same reference axis system following the procedure illustrated by Fig. 2. The starting point is the tetrahedral structure depicted in Fig. 2(a) in which the two H atoms (D atoms) are located at opposite corners of the upper (lower) surface of a cube with a side length of 2 centered at the origin (0,0,0), where the carbon atom is placed. Using the axis system depicted in Fig. 2(a), the (X,Y,Z) coordinates of the atoms labeled H^1, H^2, D^1, and D^2 are $(\sqrt{2},0,1)$, $(-\sqrt{2},0,1)$, $(0,\sqrt{2},-1)$, and $(0,-\sqrt{2},-1)$, respectively. Each of the four C_{2v} minimum energy structures 2–5, which have the structural parameters derived in Ref. 12, can be obtained from this reference structure by carrying out four successive operations illustrated in Figs. 2(b) and 2(c) with the example of structure 3. First, the CH_1 and CD_1 bonds are stretched by scaling their X, Y, and Z coordinates by the factor $a = 1.194$ Å$/\sqrt{3}$. Second, the CH_2 and CD_2 bonds are compressed by scaling their X, Y, and Z coordinates by the factor $b = 1.077$ Å$/\sqrt{3}$. These bond stretching and compressing operations preserve the tetrahedral angles between the bonds and result in the structure drawn in Fig. 2(b). The new coordinates of these atoms are then $(\sqrt{2}a,0,a)$, $(-\sqrt{2}b,0,b)$, $(0,\sqrt{2}a,-a)$, and $(0,-\sqrt{2}b,-b)$. Third, the CH_1 and CD_1 bonds are rotated around the axis $\overrightarrow{CH_1} \times \overrightarrow{CD_1}$ by $\gamma = 24.99°$ and $-\gamma$, respectively. Analogously, the CH_2 and CD_2 bonds are rotated around the axis $\overrightarrow{CH_2} \times \overrightarrow{CD_2}$ by $-\delta = -7.93°$ and δ, respectively. These bond rotation operations preserve the bond lengths and result in the structure depicted in Fig. 2(c). Finally, the coordinates of

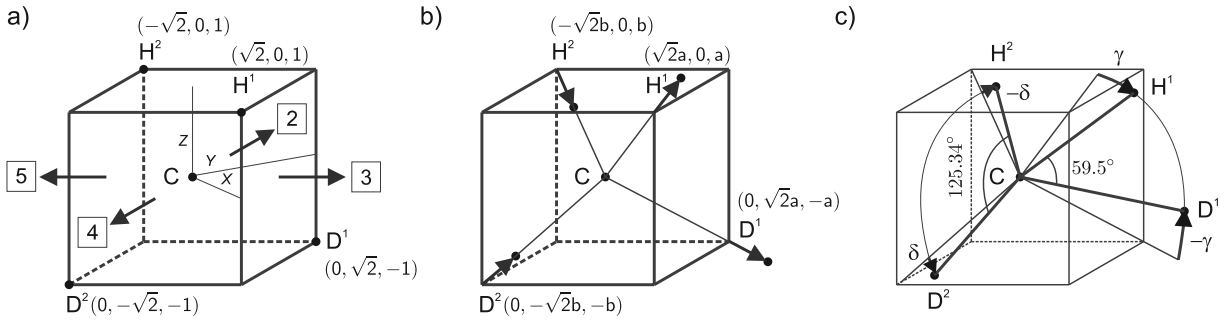

FIG. 2. (a) Space-fixed (X,Y,Z) axis system common to all four equivalent minimum energy structures of $CH_\ell H_s D_\ell D_s^+$ defined for a tetrahedral reference structure. (b) Bond-compression and bond-stretching operations and (c) bond rotations needed to convert the tetrahedral structure into the equilibrium structure 3 in Fig. 1. The arrows in (a) indicate the directions along which the bond compression, bond stretching, and bond rotations are needed to produce equilibrium structures 2–5 (see text for more details).

all atoms are shifted so that the center of mass remains at the origin of the coordinate system. All operations described above are symmetric with respect to the symmetry axis indicated by the arrow pointing toward structure 3, i.e., pointing along the (1,1,0) vector in Fig. 2(a). The other arrows pointing along the (1,−1,0), (−1,−1,0), and (−1,1,0) vectors represent schematically the equivalent set of operations necessary to form structures 4, 5, and 2, respectively.

The principal axes of inertia (c,b,a) of structure 3 can be determined from the inertial tensor determined in the reference space-fixed axis system (X,Y,Z) defined in Fig. 2(a) using Eq. (4):

$$\begin{pmatrix} I_c & & \\ & I_b & \\ & & I_a \end{pmatrix} = \mathbf{U}^\dagger \begin{pmatrix} I_{XX} & I_{XY} & I_{XZ} \\ I_{YX} & I_{YY} & I_{YZ} \\ I_{ZX} & I_{ZY} & I_{ZZ} \end{pmatrix} \mathbf{U}. \tag{4}$$

The coordinates of the five atoms $(i=1-5)$ of the C_{2v} structure 3 in the principal axis system (c,b,a) can be obtained using

$$\begin{pmatrix} i_c^{(3)} \\ i_b^{(3)} \\ i_a^{(3)} \end{pmatrix} = \mathbf{U}^\dagger \begin{pmatrix} i_X^{(3)} \\ i_Y^{(3)} \\ i_Z^{(3)} \end{pmatrix}. \tag{5}$$

Because the minimum structure 3 (and also structures 2, 4, and 5) is of C_1 symmetry, the rotational Hamiltonian cannot be simplified using symmetry arguments and is expressed as

$$\frac{\hat{H}_{\text{rot}}^{(3)}}{hc} = A^{\text{II}}\hat{J}_a^2 + B^{\text{II}}\hat{J}_b^2 + C^{\text{II}}\hat{J}_c^2 = A^{\text{II}}\sum_{\alpha,\beta} a_{\alpha\beta}^{(3)}\hat{J}_\alpha\hat{J}_\beta + B^{\text{II}}\sum_{\alpha,\beta} b_{\alpha\beta}^{(3)}\hat{J}_\alpha\hat{J}_\beta + C^{\text{II}}\sum_{\alpha,\beta} c_{\alpha\beta}^{(3)}\hat{J}_\alpha\hat{J}_\beta, \tag{6}$$

where $\alpha,\beta=X,Y,Z$ and the numerical expansion coefficients $a_{\alpha\beta}^{(3)}$, $b_{\alpha\beta}^{(3)}$, and $c_{\alpha\beta}^{(3)}$ are obtained using the coordinate transformation,

$$\begin{pmatrix} \hat{J}_c \\ \hat{J}_b \\ \hat{J}_a \end{pmatrix} = \mathbf{U}^\dagger \begin{pmatrix} \hat{J}_X \\ \hat{J}_Y \\ \hat{J}_Z \end{pmatrix}. \tag{7}$$

The numerical values of the coefficients $a_{\alpha\beta}^{(3)}$, $b_{\alpha\beta}^{(3)}$, and $c_{\alpha\beta}^{(3)}$ introduced in Eq. (6) are listed in Table I, and $a_{\alpha\beta}=a_{\beta\alpha}$, $b_{\alpha\beta}=b_{\beta\alpha}$, and $c_{\alpha\beta}=c_{\beta\alpha}$. The rotational Hamiltonians of the other structures corresponding to $CH_\ell H_s D_\ell D_s^+$ (i.e., structures 2, 4, and 5 in Fig. 1) can be derived in an analogous manner as explained above for structure 3, but following the operations depicted schematically by the distortion arrows described above. Comparing structures 2, 4, and 5 depicted in Fig. 1 with that displayed in Fig. 2(a) and considering the direction of the distortion arrows in Fig. 2(a) lead to the conclusion that it suffices to make the appropriate sign changes in the X and Y coordinates. These sign changes are summarized in Table II. The absolute values of the coefficients $a_{\alpha\beta}^{(3)}$, $b_{\alpha\beta}^{(3)}$, and $c_{\alpha\beta}^{(3)}$ of Table I thus remain unchanged for the other minimum structures, but their signs change according to the change of sign of $\alpha\beta$ evaluated using Table II. For example, $a_{XY}^{(3)}=-a_{XY}^{(4)}=a_{XY}^{(5)}=-a_{XY}^{(2)}$.

The rovibronic eigenstates of the six lowest-lying tunneling states of $CH_2D_2^+$ are obtained by diagonalizing the total Hamiltonian,

TABLE I. Numerical values of the expansion coefficients $a_{\alpha\beta}^{(3)}$, $b_{\alpha\beta}^{(3)}$, and $c_{\alpha\beta}^{(3)}$ of the rotational Hamiltonian corresponding to the minimum energy structure 3 of $CH_2D_2^+$.

$\alpha\beta$	$a_{\alpha\beta}^{(3)}$	$b_{\alpha\beta}^{(3)}$	$c_{\alpha\beta}^{(3)}$
XX	0.147 432	0.427 021	0.425 548
YY	0.834 32	0.027 375 3	0.138 305
ZZ	0.018 248 8	0.545 604	0.436 147
XY	0.350 721	−0.108 119	−0.242 601
XZ	0.051 869 6	−0.482 684	0.430 815
YZ	0.123 391	0.122 213	−0.245 604

TABLE II. Signs of the distortions along the X and Y directions needed to obtain the appropriate geometric structures of the minima $|n\rangle=2,\ldots,5$ of $CH_2D_2^+$.

$\|2\rangle$	$-X$	Y
$\|3\rangle$	X	Y
$\|4\rangle$	X	$-Y$
$\|5\rangle$	$-X$	$-Y$

$$\hat{H} = \hat{H}_{\text{tun}} + \hat{H}_{\text{rot}}, \tag{8}$$

which is block diagonal both in J and in the distinct types of minimum structures I, II, and III. For example, for $J=0$, $\hat{H}$ equals $\hat{H}_{\text{tun}}$ of Eq. (1). For $J=1$, the dimensionality of $\hat{H}$ is 18×18. The 3×3 block corresponding to $CH_\ell H_\ell D_s D_s^+$ is the $J=1$ block of the rotational Hamiltonian of Eq. (2) and the 3×3 block corresponding to $CH_s H_s D_\ell D_\ell^+$ is the $J=1$ block of the rotational Hamiltonian of Eq. (3) to which Δ' is added to each diagonal element. The four 3×3 diagonal blocks of the matrix describing the structures $CH_\ell H_s D_\ell D_s^+$ correspond to the $J=1$ block of Eq. (6) to which $\Delta\cdot\mathbb{1}$ has been added. The off-diagonal blocks connecting structures 2 and 4 and 3 and 5 are zero, whereas those connecting structures 2 and 3, 2 and 5, 3 and 4, and 4 and 5 have the form $\pm\sigma\cdot\mathbb{1}$ and reflect the connectivity of the tunneling paths indicated by the full arrows in Fig. 1. This choice is equivalent to neglecting a possible dependence of the tunneling matrix elements on the rotational angular momentum.

IV. RESULTS AND DISCUSSION

The model presented in the previous section enables one to predict the rotational-tunneling structure of the lowest three bands of the photoelectron spectrum of CH_2D_2 as a function of 13 parameters. The adiabatic ionization energy E_I, which gives the position of the ground state of the energetically most stable isomeric form of $CH_2D_2^+$, $CH_\ell H_\ell D_s D_s^+$, with respect to that of the ground state of CH_2D_2, two zero-point energy differences Δ and Δ' between $CH_\ell H_\ell D_s D_s^+$ and the isomeric forms $CH_\ell H_s D_\ell D_s^+$ and $CH_s H_s D_\ell D_\ell^+$, respectively, a tunneling matrix element σ and three rigid-rotor rotational constants per isomeric form. The C_{2v} minimum energy structure of $CH_2D_2^+$ reported in Ref. 12 was used to calculate the nine rigid-rotor rotational constants for the three isomeric forms of $CH_2D_2^+$ listed in the lower half of Table III. No attempt was made to obtain better values for these constants in the present work. Moreover, the adiabatic ionization energy E_I was kept fixed at the value determined in Ref. 12 and only three parameters, Δ, Δ', and σ, were adjusted.

TABLE III. Molecular constants describing the structure and tunneling dynamics at low energies in the $\tilde{X}^+\,{}^2B_2$ ground state of $CH_2D_2^+$.

[cm^{-1}]	I	II	III
E_I	101 852.3(14)[a]		
Δ, Δ'		123.6(5)	243.2(5)
σ		−1.7(4)	
A	4.37(3)[a]	4.91	5.17
B	3.84(4)[a]	3.31	2.97
C	2.47(3)[a]	2.53	2.76

[a]From Ref. 12.

The assumption that the zero-point energy differences are much larger than the tunneling matrix elements in Eq. (1)

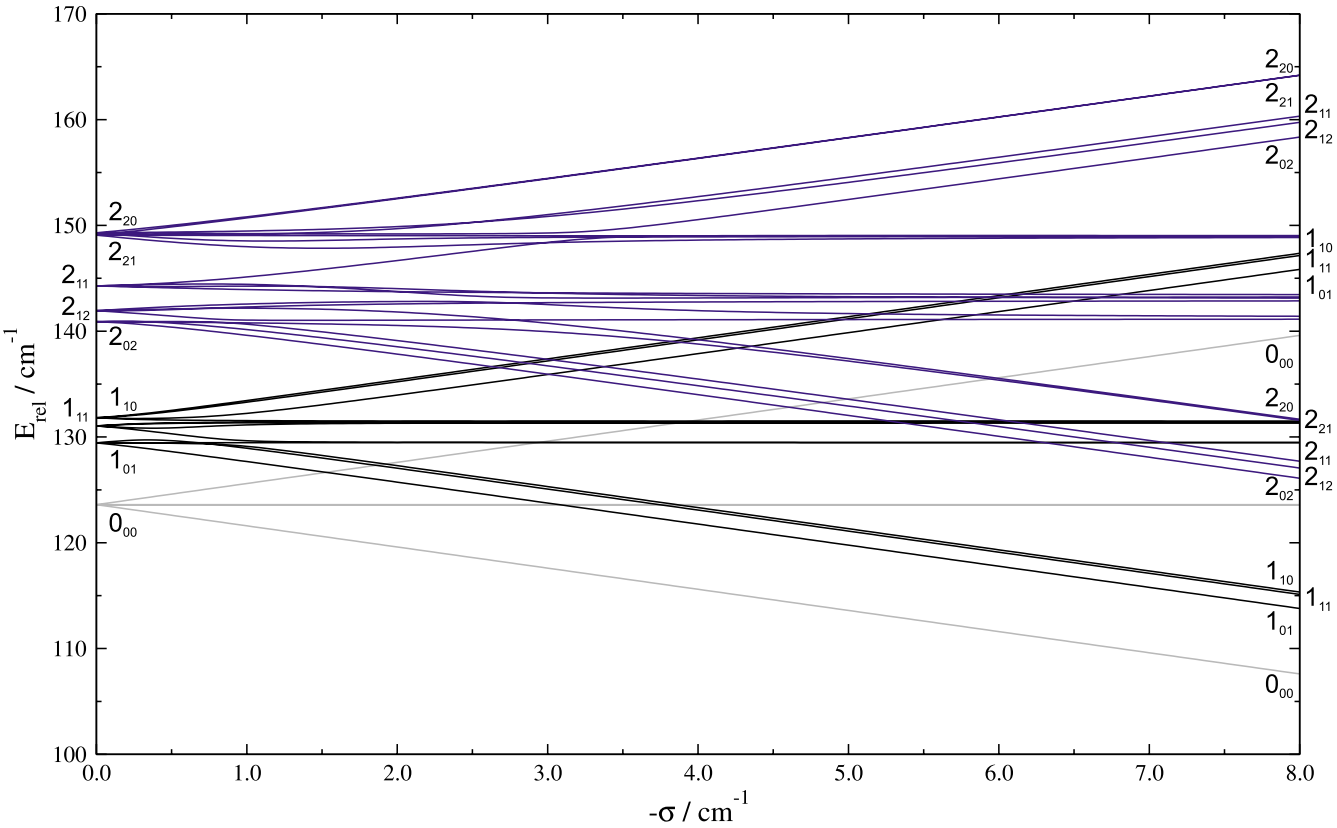

FIG. 3. Correlation diagram illustrating the effect of the tunneling matrix element σ on the energy level structure of $CH_\ell H_s D_\ell D_s^+$. The left-hand side ($\sigma=0$) corresponds to a fourfold degenerate asymmetric top of C_1 symmetry. The right-hand side ($\sigma=-8$ cm^{-1}) corresponds to a near prolate symmetric top corresponding to a tunneling wave function delocalized over the four C_{2v} equilibrium structures 2–5 of $CH_\ell H_s D_\ell D_s^+$ in Fig. 1. The asymmetric-top rotational labels are given in the notation $N^+_{K_a^+K_c^+}$.

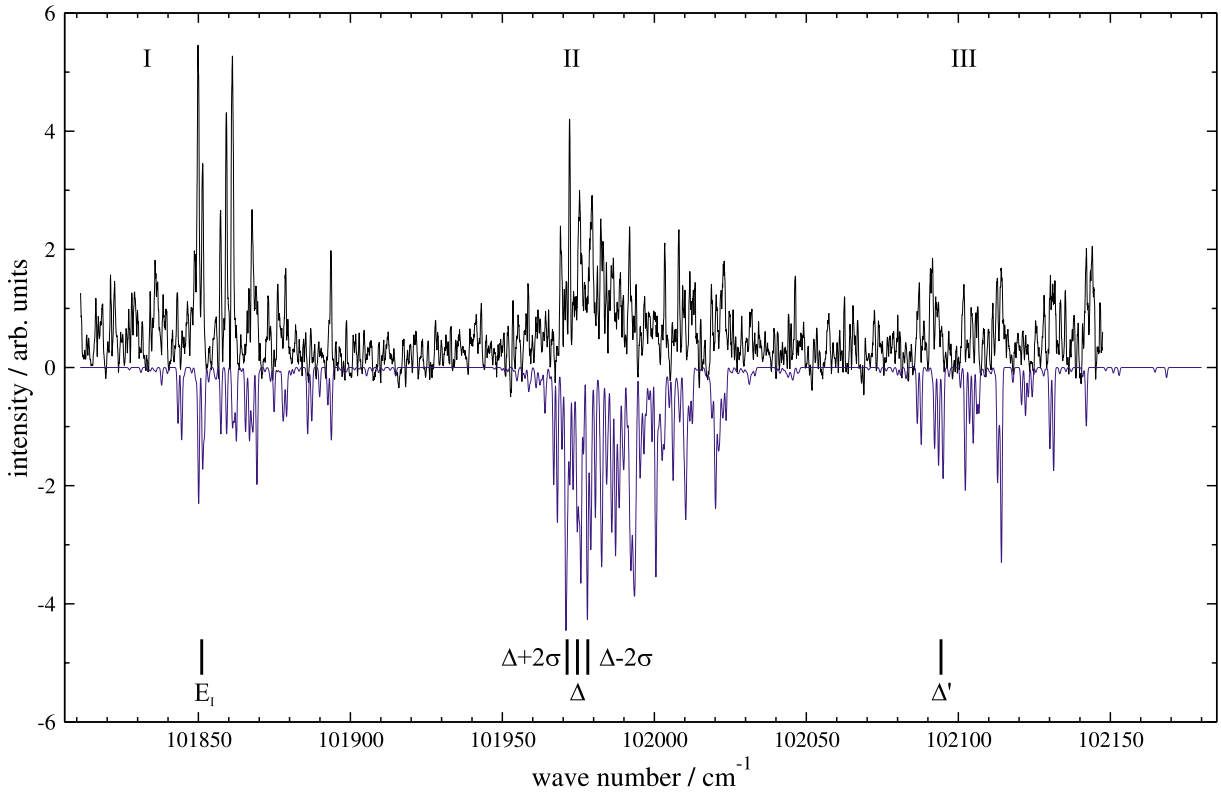

FIG. 4. Upper trace: PFI-ZEKE photoelectron spectrum of the lowest three bands of the $CH_2D_2^+$ $\tilde{X}^+\,^2B_2 \leftarrow CH_2D_2$ $\tilde{X}\,^1A_1$ transition. Lower inverted trace: Simulation based on an effective tunneling-rotational Hamiltonian (see text for more details). The positions of the band centers (including tunneling splittings) of the three isomeric forms $CH_\ell H_\ell D_s D_s^+$, $CH_\ell H_s D_\ell D_s^+$, and $CH_s H_s D_\ell D_\ell^+$ are indicated at the bottom of the figure.

enables one to treat the three isomeric forms separately and the rotational structure of $CH_\ell H_\ell D_s D_s^+$ and $CH_s H_s D_\ell D_\ell^+$ in the rigid-rotor approximation. The tunneling motion only affects the energy level structure of $CH_\ell H_s D_\ell D_s^+$ and Fig. 3 shows how this structure evolves as a function of the value of the tunneling matrix elements σ. For $\sigma=0$ (left-hand side of Fig. 3), the tunneling motion is suppressed and the level structure corresponds to that of an asymmetric top of C_1 symmetry, each level having fourfold degeneracy resulting from the four equivalent structures 2–5 in Fig. 1. This degeneracy is partially lifted when σ increases. The four $J=0$ levels split into an A_1 component of energy $\Delta+2\sigma$ (ground state), a doubly degenerate B_1+B_2 component of energy Δ, and an A_2 component of energy $\Delta-2\sigma$ (σ has a negative value[21]). A similar pattern is observed for all other asymmetric top energy levels, with the appropriate change in rovibronic symmetry. In the limit where the tunneling splittings become larger than the rotational spacings (i.e., when $|\sigma| > 4.5$ cm^{-1} for the $J \leq 1$ levels, see Fig. 3), the energy level pattern starts resembling that of three distinct vibronic (tunneling) components with the rotational constants $A \cong 4.54$ cm^{-1}, $B \cong 3.2$ cm^{-1}, and $C \cong 3.0$ cm^{-1} corresponding to a near-prolate asymmetric top. For values of σ between these limits, levels of the same J value and rovibronic symmetry repel each other and form a complex network of avoided crossings, e.g., around $\sigma=-0.8$ cm^{-1} for $J=1$ and around $\sigma=-1.5$ cm^{-1} for $J=2$. Moreover, the fact that different rotational levels of the two degenerate middle vibronic components (see left of Fig. 1) with the same rovibronic symmetry can interact within our model leads to a more complex pattern for these components.

An overview of the PFI-ZEKE photoelectron spectrum of CH_2D_2 in the region of the lowest three bands is displayed in Fig. 4, where it is compared with the results of a calculation made on the basis of the model presented in Sec. III. The overall structure of this spectrum, with a spectrally congested central band surrounded by two spectrally less dense bands, directly supports the predictions of the vibronic model displayed schematically on the left-hand side of Fig. 1. The three bands are thus assigned, in order of increasing energy, to transitions to the ground state of $CH_\ell H_\ell D_s D_s^+$, $CH_\ell H_s D_\ell D_s^+$, and $CH_s H_s D_\ell D_\ell^+$ and are displayed on an enlarged scale in Fig. 5, where the spectrum of the lowest band corresponds to a high-resolution recording.[12]

The rotational structure of the lowest band was analyzed in Ref. 12, which also reported the value of the adiabatic ionization energy, rigid-rotor rotational constants, and structural parameters for the C_{2v} equilibrium geometry, which were adopted in the present analysis (see above and second column of Table III). To calculate the spectrum displayed as inverted traces in Figs. 4 and 5, a rotational temperature of 7 K was assumed for the $\tilde{X}\,^1A_1$ ground state of CH_2D_2 and the rotational constants for this state were taken from Ref. 23. The intensities of rotational branches with $\Delta N=N^+-J''=0$, ± 1, and ± 2 were weighted by the factors 1, 0.75, and 0.5,

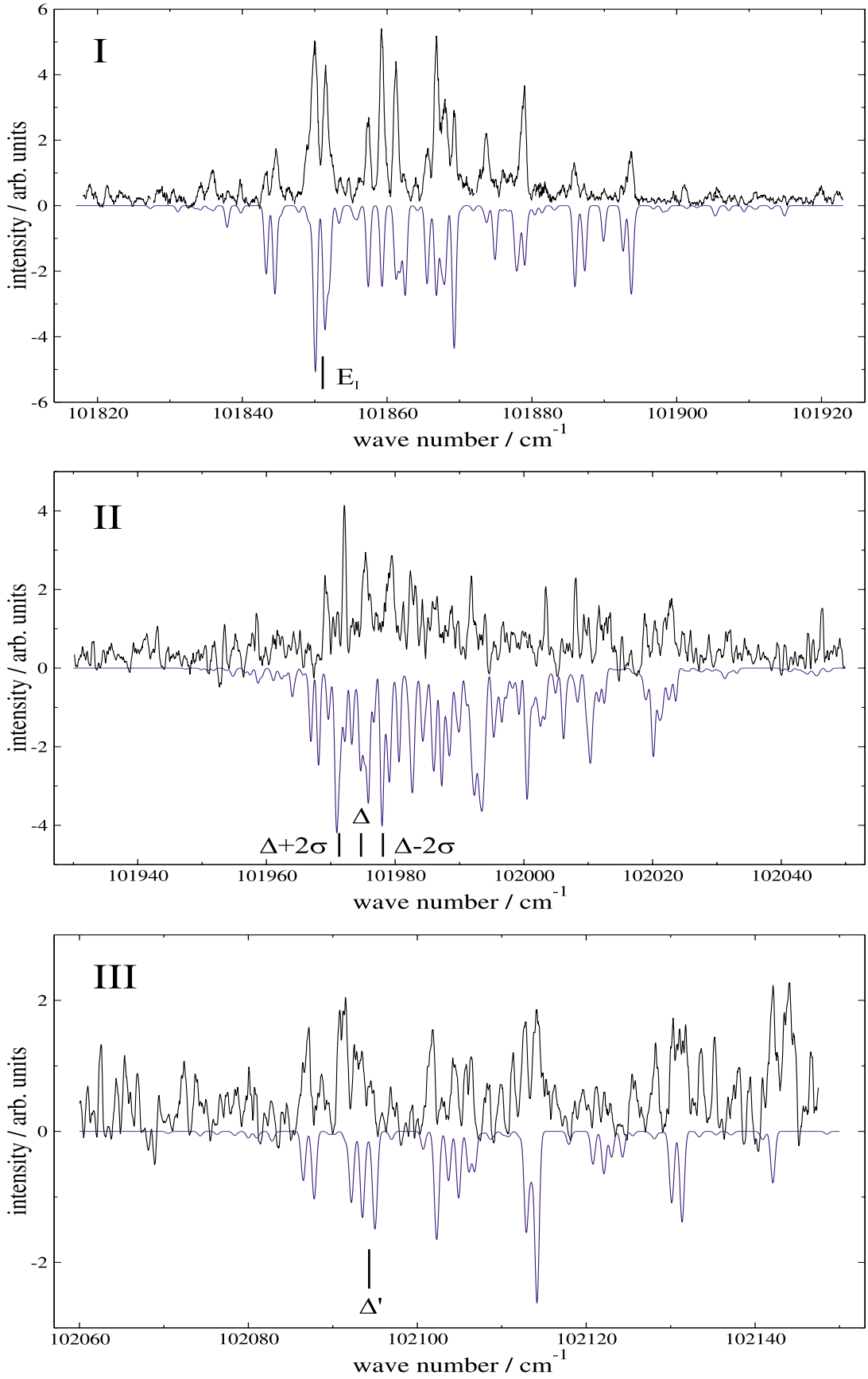

FIG. 5. Detailed view of the experimental spectra of the three lowest vibronic bands of $CH_2D_2^+$ and the corresponding simulations (inverted traces). The experimental spectrum of higher resolution shown in the top panel was taken from Ref. 12. The top, middle, and bottom panels show the rotational structure of the bands assigned to transitions to the ground states of $CH_\ell H_\ell D_s D_s^+$, $CH_\ell H_s D_\ell D_s^+$, and $CH_s H_s D_\ell D_\ell^+$, respectively. The calculated positions of the band centers (including tunneling splittings) are indicated at the bottom of each panel.

respectively, and only transitions obeying the general rovibronic photoionization selection rules of Ref. 24, i.e., $A_1 \leftrightarrow A_2$ and $B_1 \leftrightarrow B_2$ for even-ℓ photoelectron partial waves, and $A_1 \leftrightarrow A_1$, $A_2 \leftrightarrow A_2$, $B_1 \leftrightarrow B_1$, and $B_2 \leftrightarrow B_2$ for odd-ℓ photoelectron partial waves were retained as suggested by the previous study.[12] For simplicity, the intensities of transitions associated with emission of even-ℓ and odd-ℓ partial wave components were weighted equally. This choice differs from that made in Ref. 12.

The calculated spectra displayed as inverted traces in Figs. 4 and 5 were obtained by solely adjusting three parameters, the differences Δ and Δ' in zero-point energies and the tunneling matrix element σ, all other parameters remaining fixed at the values given in Table III. The calculated spectra reproduce the main features of the experimental spectra satisfactorily: Whereas the calculated and measured line positions of the lowest and highest bands are in good agreement, the intensities of several lines differ noticeably. We attribute these deviations to the simplicity of the model used to determine the line intensities, in particular to the fact that transitions leading to even-ℓ and odd-ℓ photoelectron partial waves were weighted equally and that channel interactions were neglected although they are known to influence the intensity distributions of PFI-ZEKE photoelectron spectra.[25] The observation that several lines on the high wave number side of the highest-frequency band are not reproduced in the calculation reflects the fact that this band partially overlaps with the next band in the photoelectron spectrum. The exact match of the positions of most lines of the experimental and calculated spectra of the first and third bands suggests that the rigid-rotor constants in Table III are adequate and confirm the interpretation of the lowest bands of the photoelectron spectrum in terms of three isomeric forms of $CH_2D_2^+$.

The congested and not fully resolved nature of the middle band, which corresponds to the isomeric form $CH_\ell H_s D_\ell D_s^+$, prevents a line-by-line comparison of the calculated and experimental spectra. Nevertheless, the overall band shape and the spectral density are well reproduced by the calculations, which also predict clusters of lines at the positions where these are observed experimentally, e.g., around 101 992, 102 012, and 102 023 cm^{-1}. Given that only two parameters were adjusted for this band (σ and Δ), the overall agreement between experimental and calculated spectra makes us confident that the tunneling-rotational model presented in Sec. III adequately describes the main aspects of the energy level structure of $CH_2D_2^+$ at low energies and of the tunneling dynamics of the $CH_\ell H_s D_\ell D_s^+$ isomeric form.

V. CONCLUSIONS

The analysis of the lowest three bands in the PFI-ZEKE photoelectron spectrum of CH_2D_2 completes our investigations of the rotational-tunneling energy level structure of the methane cation and its deuterated isotopomers at low energies.[11–17,21] The effective tunneling-rotation Hamiltonian used to analyze the spectra, though relatively simple, offered the advantage of a global interpretation of the spectra of all isotopomers and enabled us to interpret the low-lying bands in the photoelectron spectra of the partially deuterated isotopomers as arising from distinct isomeric forms. The zero-point energy differences $\Delta = 123.6(5)$ cm^{-1} between $CH_\ell H_\ell D_s D_s^+$ and $CH_\ell H_s D_\ell D_s^+$ and $\Delta' = 243.2(5)$ cm^{-1} between $CH_\ell H_\ell D_s D_s^+$ and $CH_s H_s D_\ell D_\ell^+$ are in good agreement with the values of 115 cm^{-1} (114 cm^{-1}) and 220 cm^{-1} (217 cm^{-1}) estimated in *ab initio* quantum chemical calculations at the UMP2/cc-pVDZ level of theory[21] [UMP2/6-31G** (Ref. 13)]. Moreover, the optimal value of the tunneling matrix elements $\sigma = -1.7(4)$ cm^{-1} fits well in the sequence of values determined for the other isotopomers of CH_4^+ [CH_4^+: $\sigma = -4.1(10)$ cm^{-1},[15] $CH_3D_s^+$: $\sigma = -3.2(2)$ cm^{-1},[17] $CH_3D_\ell^+$: $\sigma = -2.2(2)$,[17] $CD_3H_\ell^+$: $\sigma = -0.4(2)$ cm^{-1},[17] $CD_3H_s^+$: $\sigma = -0.6(1)$ cm^{-1},[17] and CD_4^+: $\sigma = -0.35(8)$ cm^{-1} (Ref. 16)] and confirms the expectation that the tunneling splittings should decrease with increasing degree of deuteration. The present analysis confirms the existence of three isomeric forms first proposed in Refs. 12 and 13.

In the future it would be desirable to obtain PFI-ZEKE photoelectron spectra with higher spectral resolution and signal-to-noise ratio, particularly for the second, spectrally dense band corresponding to the $CH_\ell H_s D_\ell D_s^+$ isomeric form that is subject to tunneling. The theoretical treatment would also gain from the inclusion of additional terms, such as Coriolis and anharmonic coupling terms, in the tunneling-rotational Hamiltonian, which currently only contains terms quadratic in the rotational angular momentum quantum number (see Ref. 16).

ACKNOWLEDGMENTS

We thank Professor R. Signorell and Dr. M. Sommavilla for their early contributions to these studies. This work was supported financially by the Swiss National Science Foundation under Project No. 200020-125030.

[1] I. B. Bersuker, Sov. Phys. JETP **16**, 933 (1963).
[2] I. B. Bersuker, *The Jahn-Teller Effect* (Cambridge University Press, Cambridge, UK, 2006).
[3] H. Köppel, W. Domcke, and L. S. Cederbaum, Adv. Chem. Phys. **57**, 59 (1984).
[4] R. F. Frey and E. R. Davidson, J. Chem. Phys. **88**, 1775 (1988).
[5] W. Meyer, J. Chem. Phys. **58**, 1017 (1973).
[6] M. N. Paddon-Row, D. J. Fox, J. A. Pople, K. N. Houk, and D. W. Pratt, J. Am. Chem. Soc. **107**, 7696 (1985).
[7] X. G. Wang and T. Carrington, Jr., J. Chem. Phys. **119**, 101 (2003).
[8] X. G. Wang and T. Carrington, J. Chem. Phys. **129**, 234102 (2008).
[9] J. W. Rabalais, T. Bergmark, L. O. Werme, L. Karlsson, and K. Siegbahn, Phys. Scr. **3**, 13 (1971).
[10] A. W. Potts and W. C. Price, Proc. R. Soc. London, Ser. A **326**, 165 (1972).
[11] R. Signorell and F. Merkt, J. Chem. Phys. **110**, 2309 (1999).
[12] R. Signorell, M. Sommavilla, and F. Merkt, Chem. Phys. Lett. **312**, 139 (1999).
[13] R. Signorell and F. Merkt, Faraday Discuss. **115**, 205 (2000).
[14] R. Signorell and M. Sommavilla, J. Electron Spectrosc. Relat. Phenom. **108**, 169 (2000).
[15] H. J. Wörner, R. van der Veen, and F. Merkt, Phys. Rev. Lett. **97**, 173003 (2006).
[16] H. J. Wörner, X. Qian, and F. Merkt, J. Chem. Phys. **126**, 144305 (2007).

[17] H. J. Wörner and F. Merkt, J. Chem. Phys. **126**, 154304 (2007).
[18] L. B. Knight, Jr., J. Steadman, D. Feller, and E. R. Davidson, J. Am. Chem. Soc. **106**, 3700 (1984).
[19] M. Matsushita, T. Momose, T. Shida, and L. B. Knight, Jr., J. Chem. Phys. **103**, 3367 (1995).
[20] L. B. Knight, Jr., G. M. King, J. T. Petty, M. Matsushita, T. Momose, and T. Shida, J. Chem. Phys. **103**, 3377 (1995).
[21] H. J. Wörner and F. Merkt, "Jahn-Teller effects in molecular cations studied by photoelectron spectroscopy and group theory," Angew. Chem., Int. Ed. Engl. (in press).
[22] I. B. Bersuker and V. Z. Polinger, Sov. Phys. JETP **39**, 1023 (1974).
[23] J. C. Deroche and G. Guelachvili, J. Mol. Spectrosc. **56**, 76 (1975).
[24] R. Signorell and F. Merkt, Mol. Phys. **92**, 793 (1997).
[25] F. Merkt and T. P. Softley, Int. Rev. Phys. Chem. **12**, 205 (1993).